

Phase changings in the surface layers of T_d-WTe_2 driven by alkali-metal deposition

Yu Zhu(朱玉), Zheng-Guo Wang(王政国), Yu-Jing Ren(任宇靖), Peng-Hao Yuan(袁鹏浩), Jing-Zhi Chen(陈景芝), Yi Ou(欧仪), Li-Li Meng(孟丽丽), and Yan Zhang(张焱)

Citation: Chin. Phys. B, 2025, 34 (**1**): 017302. DOI: 10.1088/1674-1056/ad9e9e

What follows is a list of articles you may be interested in

High-resolution angle-resolved photoemission study of large magnetoresistance topological semimetal $CaAl_4$

Xu-Chuan Wu(吴徐传), Shen Xu(徐升), Jian-Feng Zhang(张建丰), Huan Ma(马欢), Kai Liu(刘凯), Tian-Long Xia(夏天龙), and Shan-Cai Wang(王善才)

Chin. Phys. B, 2021, 30 (**9**): 097303. DOI: 10.1088/1674-1056/ac0cd7

Quantization of the band at the surface of charge density wave material 2H-$TaSe_2$

Man Li(李满), Nan Xu(徐楠), Jianfeng Zhang(张建丰), Rui Lou(娄睿), Ming Shi(史明), Lijun Li(黎丽君), Hechang Lei(雷和畅), Cedomir Petrovic, Zhonghao Liu(刘中灏), Kai Liu(刘凯), Yaobo Huang(黄耀波), and Shancai Wang(王善才)

Chin. Phys. B, 2021, 30 (**4**): 047305. DOI: 10.1088/1674-1056/abe9a8

Epitaxial fabrication of monolayer copper arsenide on Cu(111)

Shuai Zhang(张帅), Yang Song(宋洋), Jin Mei Li(李金梅), Zhenyu Wang(王振宇), Chen Liu(刘晨), Jia-Ou Wang(王嘉鸥), Lei Gao(高蕾), Jian-Chen Lu(卢建臣), Yu Yang Zhang(张余洋), Xiao Lin(林晓), Jinbo Pan(潘金波), Shi Xuan Du(杜世萱), Hong-Jun Gao(高鸿钧)

Chin. Phys. B, 2020, 29 (**7**): 077301. DOI: 10.1088/1674-1056/ab8db3

Electronic structure of correlated topological insulator candidate YbB_6 studied by photoemission and quantum oscillation

T Zhang(张腾), G Li(李岗), S C Sun(孙淑翠), N Qin(秦娜), L Kang(康璐), S H Yao(姚淑华), H M Weng(翁红明), S K Mo, L Li(李璐), Z K Liu(柳仲楷), L X Yang(杨乐仙), Y L Chen(陈宇林)

Chin. Phys. B, 2020, 29 (**1**): 017304. DOI: 10.1088/1674-1056/ab6206

Tight-binding electron-phonon coupling and band renormalization in graphene

Zhang De-Sheng (张德生), Kang Guang-Zhen (康广震), Li Jun (李俊)

Chin. Phys. B, 2015, 24 (**1**): 017301. DOI: 10.1088/1674-1056/24/1/017301

RAPID COMMUNICATION

Phase changings in the surface layers of T_d-WTe_2 driven by alkali-metal deposition

Yu Zhu(朱玉)[1], Zheng-Guo Wang(王政国)[1], Yu-Jing Ren(任宇靖)[1], Peng-Hao Yuan(袁鹏浩)[1], Jing-Zhi Chen(陈景芝)[1], Yi Ou(欧仪)[1], Li-Li Meng(孟丽丽)[1], and Yan Zhang(张焱)[1,2,†]

[1] *International Center for Quantum Materials, School of Physics, Peking University, Beijing* 100871, *China*
[2] *Collaborative Innovation Center of Quantum Matter, Beijing* 100871, *China*

(Received 23 November 2024; revised manuscript received 7 December 2024; accepted manuscript online 13 December 2024)

The discovery of phase changings in two-dimensional (2D) materials driven by external stimuli not only helps to understand the various intriguing phases in 2D materials but also provides directions for constructing new functional devices. Here, by combining angle-resolved photoemission spectroscopy (ARPES) and *in-situ* alkali-metal deposition, we studied how alkali-metal adatoms affect the electronic structure of T_d-WTe_2 on two different cleaved surfaces. We found that depending on the polarization direction of the cleaved surface, the alkali-metal deposition triggered two successive phase transitions on one surface of WTe_2, while on the other surface, no phase transition was found. We attributed the observed phase transitions to a $T_{d\uparrow}$–1T′–$T_{d\downarrow}$ structural transition driven by an alkali-metal induced sliding of WTe_2 layers. By comparing the band structure obtained in different structural phases of WTe_2, we found that the evolution of band structure across different phases is characterized by an energy scale that could be related to the degree of orbital hybridization between two adjacent WTe_2 layers. Our results demonstrate a method that manipulates the surface structure of bulk 2D materials. It also builds a direct correlation between the electronic structure and the degree of interlayer misalignment in this intriguing 2D material.

Keywords: angle-resolved photoemission spectroscopy, transition metal dichalcogenides, phase transition

PACS: 73.20.At, 77.22.Ej, 79.60.–i

DOI: 10.1088/1674-1056/ad9e9e **CSTR:** 32038.14.CPB.ad9e9e

Two-dimensional (2D) transition-metal dichalcogenides (TMD) are a large family of materials that attract great interest. Their rich and highly tunable physical properties make them promising materials for both applications and fundamental studies.[1–9] For TMD materials, the lattice structure is a critical characteristic. For example, 2H-$MoTe_2$ is an indirect gap semiconductor,[2,3] while T_d-$MoTe_2$ was proposed to be a type-II Weyl semimetal.[4,5] 2H-TaS_2 is a typical charge-density-wave (CDW) material with a 3×3 lattice period,[6] while the period of CDW in 1T-TaS_2 changes to $\sqrt{13} \times \sqrt{13}$, leading to the emergence of an intriguing insulating ground state with possible Mott and spin liquid properties.[7–9]

The close correlation between the lattice structure and electronic properties makes the discovery of phase changings in TMD materials important. In certain TMD materials where the energy difference between two structural phases is small. The phase changing from one structure to another would change the electronic properties of materials drastically.[10–16] For example, in MoS_2/$MoTe_2$, it was found that the 2H–1T or 2H–1T′ phase transition could be induced by carrier injection, tensile strain, laser irradiation, thermal annealing, etc.[11–16] Such phase transitions driven by external stimuli change the electronic property of MoS_2/$MoTe_2$ from semiconducting to metallic, which is shown to have great potential in various applications such as field-effect transistors, memory, neuromorphic computing, etc.[11–13]

Unlike other 2D TMD materials whose thermodynamically stable structures are normally 1T or 2H, the lattice structure of bulk WTe_2 is a T_d phase.[17] Each WTe_2 layer has a 1T′ structure, which can be viewed as a distorted 1T structure with a 2×1 dimerization. The T_d phase is then an orthorhombically stacking of the 1T′ WTe_2 layers. Due to its unique lattice structure, intriguing topological and electrical properties have been found in T_d-WTe_2.[18–22] Non-saturating magnetoresistance was observed in T_d-WTe_2 up to 60 T, which was explained as a perfect complementation of electrons and holes in this system.[18] It was later proposed that the bulk WTe_2 with T_d structure is a type-II Weyl semimetal exhibiting eight type-II Weyl points near the Fermi energy (E_F).[19] More intriguingly, the inversion symmetry breaks in the T_d phase, making T_d-WTe_2 one of the few 2D materials exhibiting ferroelectricity.[20,21] Ferroelectric switching driven by an electric field was found in few layers T_d-WTe_2. Such ferroelectric switching was explained as a $T_{d\uparrow}$–1T′–$T_{d\downarrow}$ phase changing due to an interlayer sliding of WTe_2 layers driven by electrostatic doping.[22]

†Corresponding author. E-mail: yzhang85@pku.edu.cn

© 2025 Chinese Physical Society and IOP Publishing Ltd. All rights, including for text and data mining, AI training, and similar technologies, are reserved.

Here, we studied the electronic structure of T_d-WTe_2 using angle-resolved photoemission spectroscopy (ARPES) and *in-situ* alkali-metal deposition. We showed that although the itinerant electrons in bulk T_d-WTe_2 screen the external electric field, phase changing could still be induced by alkali-metal deposition in the surface layers of bulk T_d-WTe_2. With the increase of alkali-metal deposition, on the sample surface with the polarization direction pointing upward ($T_{d\uparrow}$), we observed two successive transitions of electronic structure which could be attributed to the $T_{d\uparrow}$–1T′ and 1T′–$T_{d\downarrow}$ structural transitions. On the sample surface with the polarization direction pointing downward ($T_{d\downarrow}$), no transition was found. Our results highlight alkali-metal deposition as a practical method that manipulates the surface structure of bulk TMD materials. Furthermore, our data delineate the detailed evolution of electronic structure across the three different phases of WTe_2. We found an energy scale in the band structure that could be related to the degree of interlayer misalignment in T_d-WTe_2. Our results establish a correlation between the interlayer structure and electronic structure, which could be helpful for understanding the phase changes in TMD materials.

High-quality single crystals of T_d-WTe_2 were synthesized using chemical vapor transport (CVT) method.[23] Pure W powder and Te power were mixed together with the transport agent WCl_6 in a ratio of 0.93 : 2 : 0.07, and then the compound was sealed in a quartz tube. The quartz tube was put in the two-zone furnace with thermal gradient between 800 °C and 900 °C for 168 h. Then the furnace was switched off and cooled down to room temperature. ARPES measurements were performed at Peking University using a DA30L analyzer and a helium discharging lamp. The photon energy of helium lamp is 21.2 eV. The overall energy resolution was $\sim$ 12 meV and the angular resolution was $\sim 0.3°$. The crystals were cleaved *in-situ* and measured in vacuum with a base pressure better than 6×10^{-11} mbar. The experimental temperature was set to 80 K. The E_F for the samples were referenced to that of a gold crystal attached to the sample holder by Ag epoxy. The alkali-metal deposition was performed *in-situ* using a SAES potassium dispenser. The working current was set to be 6 A. For each deposition step, we only kept the potassium evaporator at the working current for 31 s to achieve a fine doping step, and then took ARPES spectra. We calculated the Fermi surface volume based on the measured band crossings. According to Luttinger's theorem, the amount of electrons deposited each step is estimated to be 7×10^{-4} electron per unit cell. Assuming each potassium atom donates one electron, each deposition step increases the alkali-metal coverage by 7×10^{-4} ML. The total alkali-metal coverage used here is estimated to be ~ 0.012 ML.

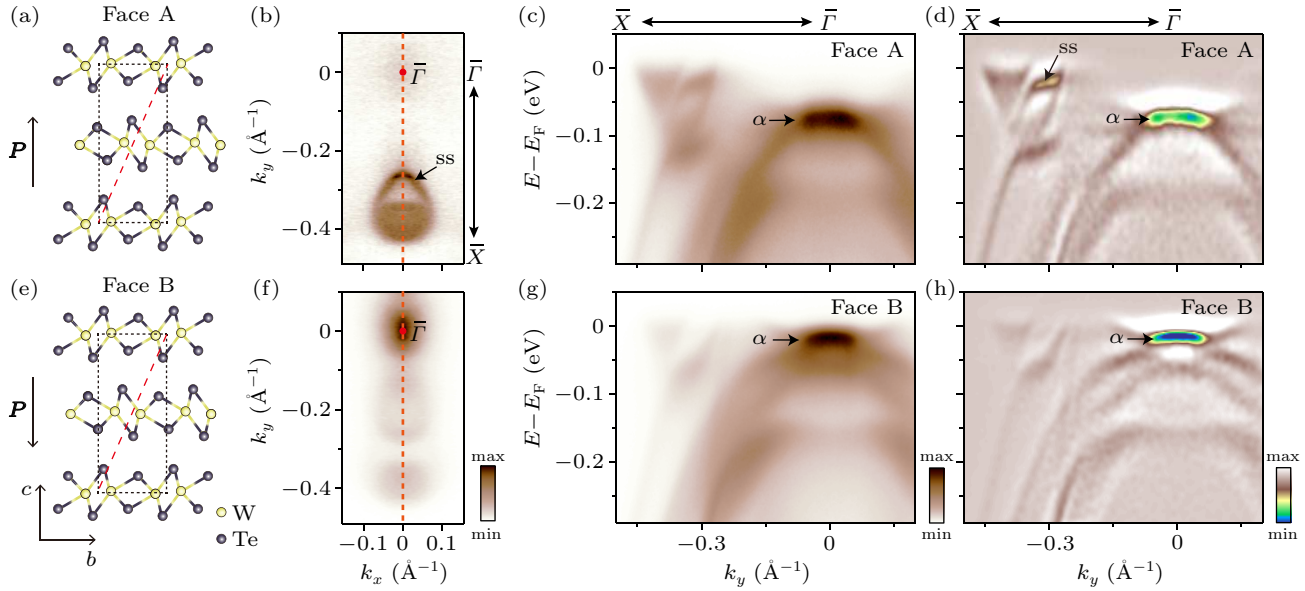


Fig. 1. Electronic structure of two different cleaved surfaces of T_d-WTe_2. (a) Lattice structure of the topmost three layers of T_d-WTe_2 with the polarization direction ($\boldsymbol{P}$) pointing upward ($T_{d\uparrow}$). (b) Fermi surface mapping taken on the $T_{d\uparrow}$ sample surface (face A). (c) Energy-momentum cut and (d) its second derivative image taken along the $\bar{X}$–$\bar{\Gamma}$ direction. The cut position is illustrated in (b) using a red dashed line. (e) Lattice structure of the topmost three layers of T_d-WTe_2 with the polarization direction pointing downward ($T_{d\downarrow}$). (f)–(h) are the same as (b)–(d) but taken on the $T_{d\downarrow}$ sample surface (face B). All data were taken at 80 K.

The lattice structure of T_d-WTe_2 is an alternate stacking of 1T′-WTe_2 layers with each layer rotating by 180° [Figs. 1(a) and 1(e)]. The space group of T_d-WTe_2 is $Pmn2_1$.[17] The inversion center of the second WTe_2 layer is misaligned with the inversion center of the first and third WTe_2 layers [Figs. 1(a) and 1(e)], which breaks the inversion symmetry of the whole material. As a result, the bulk T_d-WTe_2 has two different cleaved surfaces with the polarization direction pointing upward ($T_{d\uparrow}$) and downward ($T_{d\downarrow}$). These two cleaved surfaces can also be viewed as the front and back of the sample. In our

experiments, depending on the sample mounting directions, we could observe two different electronic states [Figs. 1(a)–1(h)] corresponding to the electronic states on the $T_{d\uparrow}$ and $T_{d\downarrow}$ sample surfaces (faces A and B), respectively. At the $\bar{\Gamma}$ point, a flat band (α) is observed at ~ -60 meV on face A [Figs. 1(c) and 1(d)], while it shifts to ~ -25 meV on face B [Figs. 1(g) and 1(h)]. Away from $\bar{\Gamma}$, an ellipse-shaped electron pocket is observed at ~ 0.4 Å^{-1} on face A. Meanwhile, a surface state (ss) that connects the hole-like band and the electron band bottom could be clearly observed.[24–27] In contrast, on face B, the surface state disappears. The electron band shifts upward and the electron pocket shrinks [Figs. 1(g) and 1(h)]. Our data are consistent with previous ARPES studies on T_d-WTe_2,[25–27] which confirms the existence of two different electronic states on the front and back surfaces of T_d-WTe_2. It has been shown that the inhomogeneous strain may also lead to the observation of different electron states on the sample surface of T_d-WTe_2.[28] However, for our experiments, the diameter of the beam spot of our helium discharging lamp is around 0.7 mm, which means that our data reflect the electronic state in the major area of the cleaved surface. The photoemission signal from the minor area of the sample surface where the inhomogeneous strain may exist cannot be observed in our experiments. Furthermore, we found that the electronic state we observed is mostly depending on the sample mount direction, but not depending on the sample cleavage. Similar data were observed repeatedly in different samples (see supplementary material for details). Therefore, our data are better explained as the different electronic states on the front and back surfaces of T_d-WTe_2 with different polarization directions. The effect of inhomogeneous strain is less relevant here.

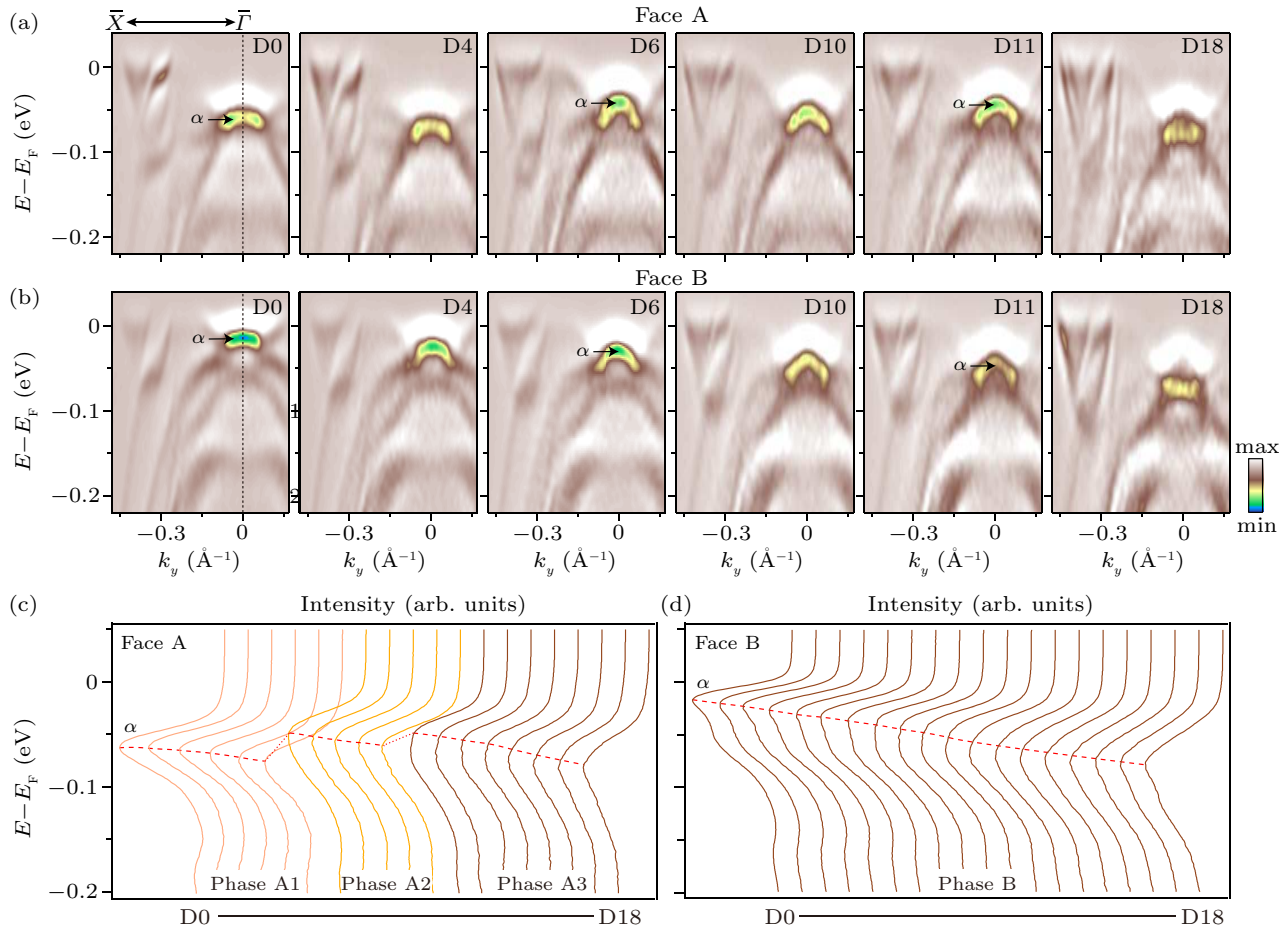


Fig. 2. Doping dependence of the electronic structure on two different cleaved surfaces of T_d-WTe_2. (a) Doping dependence of the second derivative image of the energy-momentum cut taken along the $\bar{X}$–$\bar{\Gamma}$ direction on face A. The deposition sequence is denoted using Dn. D0 refers to the pristine sample. (b) is the same as (a) but taken on face B. To check the spectral images taken in other dopings, see supplementary material for details. (c) Doping dependence of the energy-distribution-curves (EDCs) taken at the $\bar{\Gamma}$ point on face A. The position of the EDCs is illustrated in (a) using a black dashed line. Red dashed lines illustrate the energy shift of the α band position. (d) is the same as (c) but taken on face B.

We then studied how the surface deposition of alkali-metal affects the electronic states on two different cleaved surfaces of T_d-WTe_2. We repeated the same deposition procedure several times. We use Dn to denote the deposition sequence. As shown in Fig. 2, the doping dependent data taken on faces A and B behave very differently. We use the α band at the $\bar{\Gamma}$ point as a reference. The energy position of the α band can be extracted from both the minimum value of the

second derivative images [Figs. 2(a) and 2(b)] and the peak position of the EDCs [Figs. 2(c) and 2(d)]. On face A, we observed two abrupt changes of the α band position during the doping process. The α band first moves gradually towards higher binding energy with the increase of alkali-metal deposition. This is expected as the alkali-metal deposition dopes electrons into the sample surface. However, at D6 and D11, the α band shifts abruptly towards E_F. It is worth noting that for each doping step, the deposition time and measurement procedure were kept the same. Moreover, the abrupt changes of the α band position were observed reproducibly on different samples. Therefore, the non-monotonic energy shift of the α band cannot be attributed to the desorption of alkali-metal or the degradation of the sample surface. Our observation indicates that the alkali-metal deposition drives two successive phase transitions of electronic state on face A. In contrast to the transitions observed on the $T_{d\uparrow}$ sample surface, the evolution of the electronic state on face B is continuous. The α band shifts monotonically towards higher binding energy with the increase of alkali-metal deposition.

For the convenience of our discussion, we name the three different phases observed on face A phase A1, A2, and A3 respectively, and the electronic phase observed on face B phase B [Figs. 2(c) and 2(d)]. We then compare the band structure observed in different phases in Fig. 3. In phase A1 [Fig. 3(a)], four bands could be resolved near ~ -0.3 Å^{-1}, including two electron-like bands (δ and γ), one hole-like band (β), and one surface band (ss). The inflection point of ss is at ~ 20 meV below E_F. The inflection point of β is at ~ -120 meV, which is below the γ band bottom. When entering the phase A2 [Fig. 3(b)], depending on the band shift direction, the observed low-energy bands of T_d-WTe_2 can be divided into two groups. δ and γ shift towards higher binding energy. The γ band bottom shifts to ~ 120 meV below E_F. However, for the β and ss bands, they shift towards the opposite direction. The ss band moves closer to E_F. The inflection point of β shifts to ~ -100 meV which is now above the γ band bottom. We could use the energy separation between the ss and γ bands at -0.3 Å^{-1} (ΔE) to describe the relative energy shift between the two groups of bands. When the system transits from phase A1 to A2, ΔE increases significantly. However, when entering phase A3 [Fig. 3(c)], ΔE declines. The two groups of bands shift towards each other. The inflection point of the ss band shifts back to ~ 20 meV below E_F. The inflection point of β and the band bottom of γ are now very close, which is manifested as one broad peak in the EDCs [Fig. 3(d)].

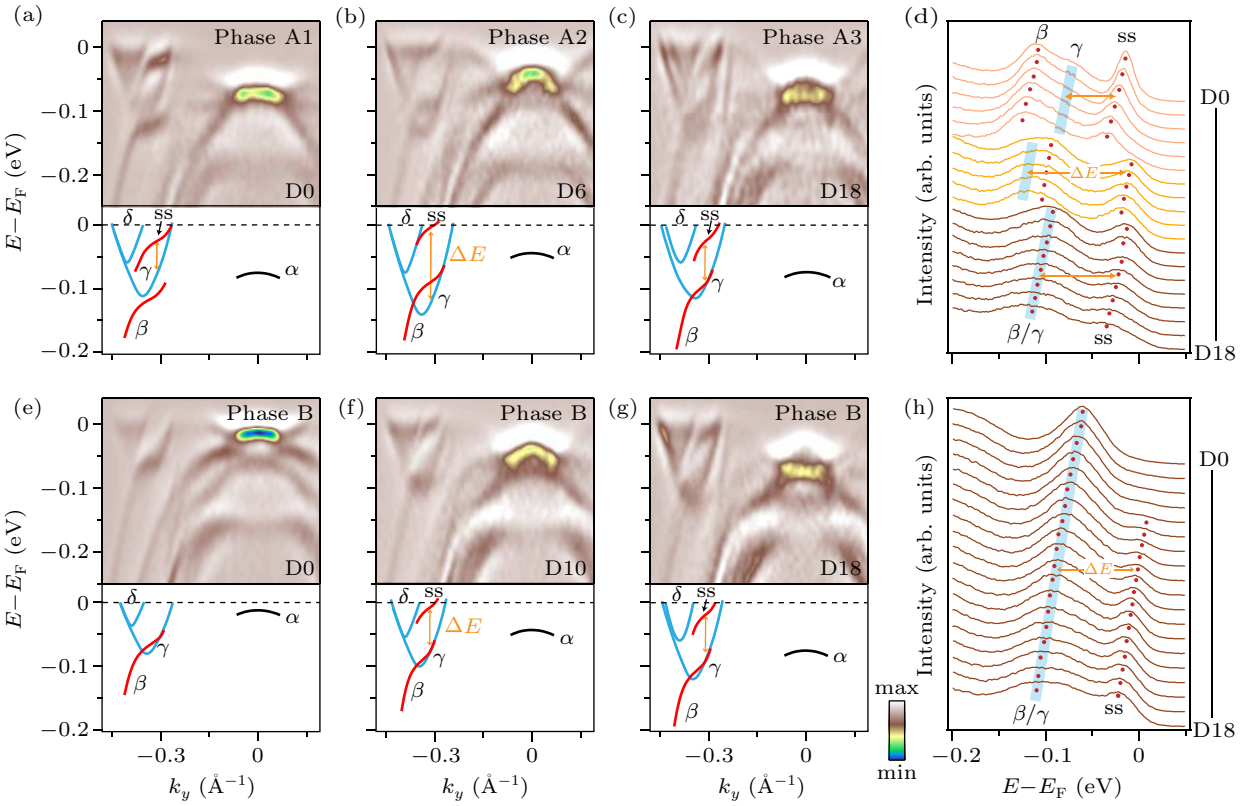


Fig. 3. The band structures taken in different electronic phases of alkali-metal deposited T_d-WTe_2. (a) Second derivative image of the energy-momentum cut taken along the $\bar{X}$–$\bar{\Gamma}$ direction on face A. The bottom panel illustrates the band dispersions extracted from the second derivative image. The data were taken in the phase A1 in the pristine sample (D0). (b) and (c) are the same as (a) but taken in phases A2 and A3 in D6 and D18 samples, respectively. (d) Doping dependence of the EDC taken at -0.3 Å^{-1} on face A. The red circles illustrate the band positions of β and ss. The blue translucent lines are the guides to the eye to illustrate the band positions of γ. (e), (f), and (g) are the same as (a) but taken on face B in D0, D10 and D18 samples, respectively. (h) is the same as (d) but taken on face B.

For the phase B on the $T_{d\downarrow}$ sample surface [Figs. 3(e)–3(h)], the electron-like bands δ and γ shift monotonically towards higher binding energy. The inflection point of β is close to the γ band bottom. The surface band ss is above E_F in the undoped sample [Fig. 3(e)], and thereby cannot be observed. It shifts below E_F at D4 and then moves monotonically towards higher binding energy with the increase of alkali-metal deposition. No abrupt change of ΔE was observed in the doping dependence of band structure taken on face B.

Based on the analyses of the bands near $\bar{\Gamma}$ and -0.3 Å^{-1}, we confirmed that the alkali-metal deposition triggers two successive phase transitions on the $T_{d\uparrow}$ sample surface, while no phase transition occurs on the $T_{d\downarrow}$ sample surface. Alkali-metal deposition has been widely used in ARPES studies.[29–32] It has been shown that the alkali-metal adatoms could generate a vertical electronic field that penetrates into the sample surface.[31,32] If only the surface layers were considered, the alkali-metal deposition could cause an electrostatic doping effect similar to the gating electronic field that is applied on thin films. Therefore, we could attribute the observed two phase transitions to the $T_{d\uparrow}$–1T′–$T_{d\downarrow}$ ferroelectric switching observed in few layers T_d-WTe_2.[22] As shown in Fig. 4(a), the spontaneous polarization of the $T_{d\uparrow}$ sample surface competes with the electronic field generated by the alkali-metal adatoms. With the increase of alkali-metal deposition, the flip of polarization direction occurs between the first and second WTe_2 layers. The polarization of T_d-WTe_2 originates from the misalignment of the two adjacent WTe_2 layers.[20] Therefore, the polarization flip could be achieved by a relative sliding between the first and second WTe_2 layers. As a result, the inversion symmetry of the topmost three WTe_2 layers recovers. The stacking structure of the topmost three WTe_2 layers changes from $T_{d\uparrow}$ to 1T′. With further doping of alkali metal, the polarization flip occurs between the second and third WTe_2 layers. Together with the sliding of WTe_2 layers, the stacking structure of the topmost three WTe_2 layers changes from 1T′ to $T_{d\downarrow}$.

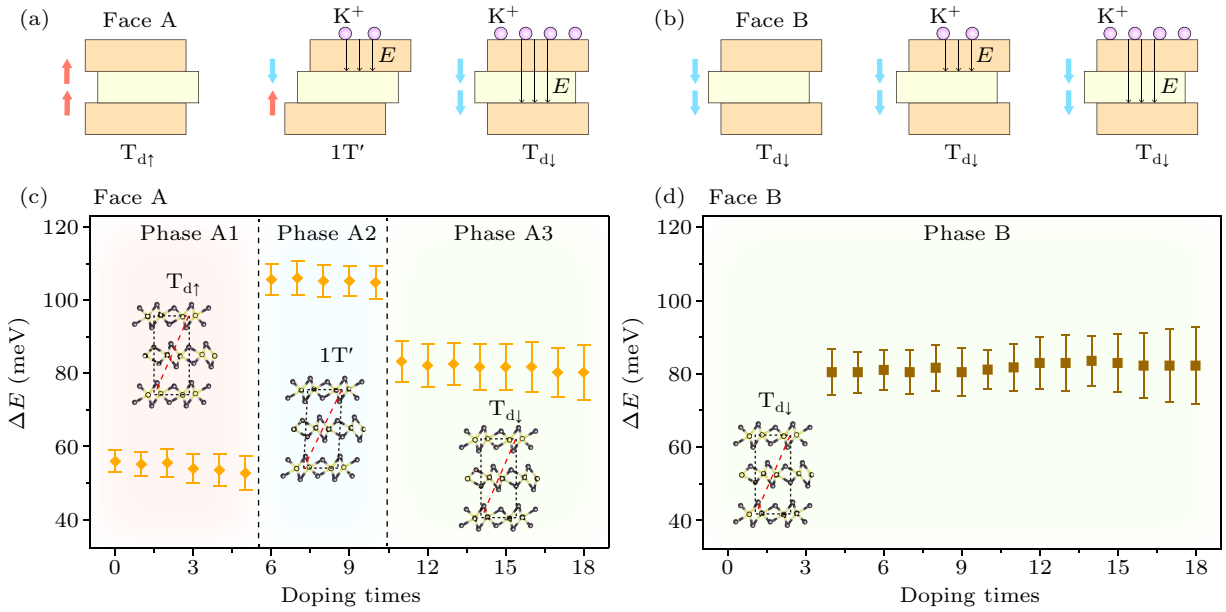


Fig. 4. Phase changings in the alkali-metal deposited T_d-WTe_2. (a) Schematic drawing of the interlayer sliding that may occur on the $T_{d\uparrow}$ sample surface with alkali-metal deposition. The orange and yellow blocks illustrate the topmost three WTe_2 layers. The red and blue arrows illustrate the polarization directions. (b) is the same as (a) but for the $T_{d\downarrow}$ sample surface. (c) Doping dependence of the energy separation between ss and γ at -0.3 Å^{-1} (ΔE) calculated based on the doping dependence data taken on face A. Schematic drawings of different stacking structures are illustrated. (d) is the same as (c) but calculated based on the data taken on face B. The error bars were estimated based on the spectral broadness of the EDCs and the second derivative images.

The $T_{d\uparrow}$–1T′–$T_{d\downarrow}$ phase changing scenario explains well the doping dependence data observed here in alkali-metal deposited T_d-WTe_2. First, the structural transition, especially the transition of stacking structure in TMD material is normally a first order transition.[33] This is consistent with the abrupt change of band positions observed in Figs. 2 and 3. Second, the $T_{d\uparrow}$–1T′–$T_{d\downarrow}$ phase changing is driven by the competition between the spontaneous polarization field of T_d-WTe_2 and the electronic field generated by the alkali-metal adatoms. This explains well the absence of phase transition on the $T_{d\downarrow}$ sample surface, where the spontaneous polarization field and the alkali-metal generated electric field are in the same direction. Third, if we treat the alkali-metal deposited surface as an infinitely large charged plate, according to Gauss's theorem, the electric field generated by the alkali-metal adatoms at D6 is around 0.17 V/nm, which is of the same order of magnitude as the gating electronic field that drives the $T_{d\uparrow}$–1T′ transition in few-layers WTe_2.[22] Fourth, if one compares

the band structures taken in phases A3 and B [Figs. 3(c) and 3(g)], it would be found that their band structures are nearly identical. This is consistent well with the ferroelectric switching scenario [Figs. 4(a) and 4(b)]. Due to the switching of polarization direction, with sufficient alkali-metal deposition, the stacking structures of the topmost three layers on faces A and B would eventually become identical. It is worth noting that considering the probe depth of APRES and the penetration depth of the alkali-metal induced electric field, a minimal model that considers only the topmost three WTe_2 layers is reasonable. However, we cannot exclude the possibility that the phase changing might involve more WTe_2 layers near the sample surface. Further experiments are required to confirm how the stacking structure changes in the surface layers of alkali-metal deposited T_d-WTe_2.

The ability to drive the phase changing of material *in-situ* enables us to study how the change of stacking structure affects the electronic structure of WTe_2. The 1T′ phase is not a thermodynamically stable phase for bulk WTe_2.[34] 1T′-WTe_2 could only be found at high temperature. Our data show that the alkali-metal deposition triggers a polarization flip in the surface layers of T_d-WTe_2, which provides an effective way to realize 1T′ phase of WTe_2 at low temperature. While T_d-WTe_2 is a Weyl semimetal, 1T′-WTe_2 is topologically trivial due to the recovery of inversion symmetry. In the early ARPES studies on T_d-WTe_2, it has been proposed that the surface state connecting the hole and electron pockets is topologically nontrivial.[24,28] The surface state was attributed to the Fermi arc that connects the two Weyl points. However, later band calculations showed that the surface state observed by ARPES could be topologically trivial. The surface state was found in the band calculations with and without the Weyl points.[25] Here, we show that the surface state could be observed in 1T′-WTe_2 [Fig. 3(b)]. Our result thus confirms that the surface state connecting the hole and electron bands in T_d-WTe_2 is topologically trivial.

In Fig. 3, we show that the bands near -0.3 Å^1 could be divided into two groups. They shift oppositely during the $T_{d\uparrow}$ to 1T′ phase transition. We then calculated the energy separation between ss and γ at -0.3 Å^{-1} (ΔE) and plotted its doping dependence in Figs. 4(c) and 4(d). We found that ΔE is closely related to the stacking structure of WTe_2. The $T_{d\uparrow}$ stacking of WTe_2 layers has the lowest ΔE (~ 55 meV), while for the $T_{d\downarrow}$ stacking of WTe_2 layers, ΔE increases to ~ 80 meV. The highest ΔE is found in the 1T′ stacking of WTe_2 layers. Its value reaches up to ~ 105 meV. According to the band calculations, the orbital characters of the low energy bands of WTe_2 are complex.[35] Many orbitals are involved including d_{z^2}, p_z, d_{xz}, and p_x orbitals. When the relative sliding of two adjacent WTe_2 layers occurs, the interlayer overlapping of orbitals changes. Depending on the different shapes of orbitals, the change of interlayer overlapping could be strongly orbital-dependent, which might lead to the band-dependent energy shifts observed here in the $T_{d\uparrow}$–1T′–$T_{d\downarrow}$ phase transitions. We note that the 1T′ stacking of WTe_2 layers pushes the two groups of bands away from each other, causing a much higher ΔE than that of the T_d stacking of WTe_2 layers, which may explain the structural instability of 1T′-WTe_2. To understand quantitatively the relation between the stacking structure and ΔE, further theoretical studies are required. Nevertheless, we show that the band structure of WTe_2 could be modulated by adjusting the degree of misalignment between two adjacent WTe_2 layers. In T_d-WTe_2, the type and number of the Weyl points are directly correlated to the band positions.[19] It is then intriguing to further study how the sliding of WTe_2 layers away from their balanced positions affects the topological and physical properties of T_d-WTe_2.

In summary, utilizing ARPES and *in-situ* alkali-metal deposition, we studied alkali-metal induced phase changings on two cleaved surfaces of T_d-WTe_2. We show that the alkali-metal deposition triggers a $T_{d\uparrow}$–1T′–$T_{d\downarrow}$ phase transition on the $T_{d\uparrow}$ sample surface of bulk WTe_2. The alkali-metal deposition could be viewed as an effective gating field, inducing an electronic field that penetrates into the surface layers of bulk materials. Our results highlight the alkali-metal deposition as an effective method that could manipulate the surface character of bulk TMD materials. The alkali-metal deposition could be used to manipulate other low-dimensional materials with spontaneous internal polarization, such as h-BN, rhombohedral-stacking WSe_2, T_d-$MoTe_2$, etc.[36–38] It is also intriguing to study the effect of hole dopants such as oxygen absorption. If an electronic field with opposite direction could be induced by the hole dopants, the switching of polarization direction may be observed in T_d-WTe_2 on face B instead of face A. Furthermore, the ability to trigger the structural transitions *in-situ* enables us to study how the change of stacking structure affects the electronic structure of TMD materials. We found that the energy shifts of bands across the structural transition are strongly band-dependent. The energy separation between certain bands could be used as an energy scale that characterizes the degree of misalignment between the WTe_2 layers. With the recent discoveries of rich phenomena in twisted bilayer or trilayer two-dimensional (2D) materials,[39,40] the understanding of the interlayer physics of 2D TMD materials becomes increasingly important. Our results provide experimental clues to understand how the form of stacking or the interlayer sliding could affect the electronic structure of 2D TMD materials.

Acknowledgments

Project supported by the National Key Research and Development Program of China (Grant No. 2022YFA1403502)

and the National Natural Science Foundation of China (Grant No. 11888101).

References

[1] Manzeli S, Ovchinnikov D, Pasquier D, Yazyev O V and Kis A 2017 *Nat. Rev. Mater.* **2** 17033

[2] Lezama I G, Arora A, Ubaldini A, Barreteau C, Giannini E, Potemski M and Morpurgo A F 2015 *Nano Lett.* **15** 2336

[3] Ruppert C, Aslan B and Heinz T F 2014 *Nano Lett.* **14** 6231

[4] Deng K, Wan G, Deng P, *et al.* 2016 *Nat. Phys.* **12** 1105

[5] Huang L, McCormick T M, Ochi M, Zhao Z, Suzuki M T, Arita R, Wu Y, Mou D, Cao H, Yan J, Trivedi N and Kaminski A 2016 *Nat. Mater.* **15** 1155

[6] Tidman J P, Singh O, Curzon A E and Frindt R F 2006 *Philos. Mag.* **30** 1191

[7] Wang Y D, Yao W L, Xin Z M, Han T T, Wang Z G, Chen L, Cai C, Li Y and Zhang Y 2020 *Nat. Commun.* **11** 4215

[8] He W Y, Xu X Y, Chen G, Law K T and Lee P A 2018 *Phys. Rev. Lett.* **121** 046401

[9] Klanjšek M, Zorko A, Žitko R, Mravlje J, Jagličić Z, Biswas Pabitra K, Prelovšek P, Mihailovic D and Arčon D 2017 *Nat. Phys.* **13** 1130

[10] Li W, Qian X and Li J 2021 *Nat. Rev. Mater.* **6** 829

[11] Kappera R, Voiry D, Yalcin S E, Branch B, Gupta G, Mohite A D and Chhowalla M 2014 *Nat. Mater.* **13** 1128

[12] Zhu X, Li D, Liang X and Lu W D 2018 *Nat. Mater.* **18** 141

[13] Hou W, Azizimanesh A, Sewaket A, Peña T, Watson C, Liu M, Askari H and Wu S M 2019 *Nat. Nanotechnol.* **14** 668

[14] Cho S, Kim S, Kim J H, Zhao J, Seok J, Keum D H, Baik J, Choe D H, Chang K J, Suenaga K, Kim S W, Lee Y H and Yang H 2015 *Science* **349** 625

[15] Wang Y, Xiao J, Zhu H, Li Y, Alsaid Y, Fong K Y, Zhou Y, Wang S, Shi W, Wang Y, Zettl A, Reed E J and Zhang X 2017 *Nature* **550** 487

[16] Keum D H, Cho S, Kim J H, Choe D H, Sung H J, Kan M, Kang H, Hwang J Y, Kim S W, Yang H, Chang K J and Lee Y H 2015 *Nat. Phys.* **11** 482

[17] Lee C H, Silva E C, Calderin L, Nguyen M A T, Hollander M J, Bersch B, Mallouk T E and Robinson J A 2015 *Sci. Rep.* **5** 10013

[18] Ali M N, Xiong J, Flynn S, Tao J, Gibson Q D, Schoop L M, Liang T, Haldolaarachchige N, Hirschberger M, Ong N P and Cava R J 2014 *Nature* **514** 205

[19] Soluyanov A A, Gresch D, Wang Z, Wu Q, Troyer M, Dai X and Bernevig B A 2015 *Nature* **527** 495

[20] Yang Q, Wu M and Li J 2018 *J. Phys. Chem. Lett.* **9** 7160

[21] Fei Z, Zhao W, Palomaki T A, Sun B, Miller M K, Zhao Z, Yan J, Xu X and Cobden D H 2018 *Nature* **560** 336

[22] Xiao J, Wang Y, Wang H, Pemmaraju C D, Wang S, Muscher P, Sie E J, Nyby C M, Devereaux T P, Qian X, Zhang X and Lindenberg A M 2020 *Nat. Phys.* **16** 1028

[23] Wang L, Gutiérrez-Lezama I, Barreteau C, Ubrig N, Giannini E and Morpurgo A F 2015 *Nat. Commun.* **6** 8892

[24] Wang C, Zhang Y, Huang J, *et al.* 2016 *Phys. Rev. B* **94** 241119

[25] Bruno F Y, Tamai A, Wu Q S, Cucchi I, Barreteau C, de la Torre A, McKeown Walker S, Ricc'o S, Wang Z, Kim T K, Hoesch M, Shi M, Plumb N C, Giannini E, Soluyanov A A and Baumberger F 2016 *Phys. Rev. B* **94** 121112

[26] Wan Y, Wang L, Kuroda K, Zhang P, Koshiishi K, Suzuki M, Kim J, Noguchi R, Bareille C, Yaji K, Harasawa A, Shin S, Cheong S W, Fujimori A and Kondo T 2022 *Phys. Rev. B* **105** 085421

[27] Rossi A, Restta G, Lee S H, Redwing R D, Jozwiak C, Bostwick A, Rotenberg E, Savrasov S Y and Vishik I M 2020 *Phys. Rev. B* **102** 121110

[28] Wu Y, Mou D, Jo N H, Sun K, Huang L, Bud'ko S L, Canfield P C and Kaminski A 2016 *Phys. Rev. B* **94** 121113

[29] Han T T, Chen L, Cai C, Wang Z G, Wang Y D, Xin Z M and Zhang Y 2021 *Phys. Rev. Lett.* **126** 106602

[30] Wang Z G, Yao W l, Wang Y D, Xin Z M, Han T T, Chen L, Ou Y, Zhu Y, Cai C, Li Y and Zhang Y 2023 *Chin. Phys. B* **32** 107404

[31] Kim J, Baik S S, Ryu S H, Sohn Y, Park S, Park B G, Denlinger J, Yi Y, Choi H J and Kim K S 2015 *Science* **349** 723

[32] Kang M, Kim B, Ryu S H, Jung S W, Kim J, Moreschini L, Jozwiak C, Rotenberg E, Bostwick A and Kim K S 2017 *Nano Lett.* **17** 1610

[33] Ji S, Grånäs O and Weissenrieder J 2021 *ACS Nano* **15** 8826

[34] Tao Y, Schneeloch J A, Aczel A A and Louca D 2020 *Phys. Rev. B* **102** 060103

[35] Kim H J, Kang S H, Hamada I and Son Y W 2017 *Phys. Rev. B* **95** 180101

[36] Li L and Wu M 2017 *ACS Nano* **11** 6382

[37] Wang X, Yasuda K, Zhang Y, Liu S, Watanabe K, Taniguchi T, Hone J, Fu L and Jarillo-Herrero P 2022 *Nat. Nanotechnol.* **17** 367

[38] Jindal A, Saha A, Li Z, Taniguchi T, Watanabe K, Hone J C, Birol T, Fernandes R M, Dean C R, Pasupathy A N and Rhodes D A 2023 *Nature* **613** 48

[39] Park J M, Cao Y, Watanabe K, Taniguchi T and Jarillo-Herrero P 2021 *Nature* **590** 249

[40] Cao Y, Fatemi V, Fang S, Watanabe K, Taniguchi T, Kaxiras E and Jarillo-Herrero P 2018 *Nature* **556** 43